Very-low-energy electron diffraction from TiS_2: experiment and *ab initio* theory

2009 J. Phys.: Condens. Matter 21 314009

(http://iopscience.iop.org/0953-8984/21/31/314009)

J. Phys.: Condens. Matter **21** (2009) 314009 (7pp) doi:10.1088/0953-8984/21/31/314009

Very-low-energy electron diffraction from TiS_2: experiment and *ab initio* theory

E E Krasovskii[1,2,3] **and V N Strocov**[4]

[1] Institute of Metal Physics, National Academy of Sciences of Ukraine, Kiev, Ukraine
[2] Departamento de Física de Materiales, Facultad de Químicas, Universidad del País Vasco, Apartado 1072, San Sebastián/Donostia, 20080 Basque Country, Spain
[3] Donostia International Physics Center (DIPC), Paseo de Manuel Lardizibal, 4 San Sebastián/Donostia, 20018 Basque Country, Spain
[4] Swiss Light Source, Paul Scherrer Institute, CH-5232 Villigen PSI, Switzerland

E-mail: eugene_krasovskii@ehu.es and vladimir.strocov@psi.ch

Received 31 December 2008, in final form 24 April 2009
Published 7 July 2009
Online at stacks.iop.org/JPhysCM/21/314009

Abstract
An experimental and theoretical study of very-low-energy electron diffraction from the (0001) surface of 1T TiS_2 is presented. The normal incidence electron transmission spectrum is measured up to 37 eV above the Fermi level. *Ab initio* calculations of the spectra are performed with the full-potential extended linear augmented plane wave $\mathbf{k}\cdot\mathbf{p}$ method. The experimental spectrum is interpreted in terms of the unoccupied complex band structure (CBS) of the semi-infinite crystal. Three CBS branches responsible for the electron transmission at normal incidence are determined. The role of inelastic scattering is discussed. The energy dependence of the optical potential V_i is determined from the shape of the experimental spectral structures. A sharp increase of V_i at 21.5 eV is detected, which is associated with a plasmon peak in the electron energy-loss function.

(Some figures in this article are in colour only in the electronic version)

1. Introduction

The rapid development of surface microscopy techniques, such as low-energy electron microscopy or scanning tunnelling microscopy, has revived interest in the physics of electron scattering by surfaces, especially at kinetic energies of a few electron volts. This regime is characterized by a reduced inelastic scattering of electrons, which makes the connection between the observed electron transmission spectra and the underlying electronic structure more transparent, and at the same time requires a very accurate treatment of the multiple scattering of incident electrons.

For periodic solids, the band structure theory is an attractive approach because it combines the computational accuracy of modern band structure methods with a convenient language for the interpretation of results, namely, the language of Bloch states. The scattering state Φ arising from an electron incident from vacuum is represented in the bulk of the crystal by a linear combination of partial waves. These waves are propagating and evanescent Bloch eigenfunctions $\psi_{k_\perp}$ of the crystal Hamiltonian comprising the *complex band structure* of the semi-infinite crystal [1]. Then the scattering problem consists in finding the coefficients of the partial waves. The Bloch wave approach to LEED was developed in the early years of LEED theory within a plane wave pseudopotential technique [2]. It was extended to all-electron potentials (i.e. the potentials with a Z/r singularity at the nucleus) in [3–5]. An alternative approach is exemplified by the layer KKR method [6], in which the crystal is represented by a *finite* number of atomic monolayers, and the multiple scattering is calculated by the Green function method. It is considered a computational advantage of this method that it avoids calculating the partial waves and proceeds immediately to the solution Φ that we seek [7]. However, as a consequence, the relation to the underlying band structure is blurred. Understanding the role of different Bloch states in transmitting the current into the crystal is especially important in view of the unavoidable shortcomings of the state-of-the-art *ab initio* theories: owing to the fundamental approximations involved in the construction of the quasiparticle Hamiltonian, we can never expect a pointwise agreement between theoretical and experimental LEED spectra. Moreover, it is our aim to infer

from the comparison with the experiment what the actual quasiparticle band structure looks like.

Apart from the explanation of electron transmission through the surface, the knowledge of unoccupied states is necessary in order to study occupied band structure by angle-resolved photoemission. A connection to VLEED is established by the one-step theory of photoemission (see, for example, [8]), in which the photoelectron final state is exactly the time-reversed LEED state. To unambiguously extract information about occupied states one needs to know both the dispersion of the final state waves in $k_\perp$ (the Bloch vector in the surface perpendicular direction) and their momentum broadening (expressed by an imaginary part of $k_\perp$). The latter determines the *intrinsic* $k_\perp$ resolution of the photoemission experiment and leads to a broadening of photoelectron spectra from the $k_\perp$-dispersive occupied states [9]. The momentum broadening is immediately connected with the inelastic scattering rate in the final state, which in the present context is quantified by the optical potential V_i, an imaginary part of the potential in the crystal. The finite photoelectron escape depth is seen as the real-space counterpart of $\mathrm{Im}\, k_\perp$, which within the one-step theory is equivalent to the mean free path of the incident electron in LEED [10].

We have performed a number of combined experimental and theoretical studies of the unoccupied band structure of layered dichalcogenides $NbSe_2$ [11] and $TiTe_2$ [12], and graphite [10]. Owing to the scattering by the interlayer potential barrier, the unoccupied energy bands of layered materials are very complicated and the target current spectra $T(E)$—transmitted current versus energy—exhibit rich structure. Based on the convincing agreement between theory and experiment we were able to extract information on the lifetimes of the final state quasiparticles from the measured broadening of the VLEED spectral structures.

In the present paper we study the unoccupied band structure of TiS_2. Similar to a number of transition metal dichalcogenides it crystallizes in the CdI_2 structure [13], which is made of hexagonal S–Ti–S sandwich layers bound by a weak van der Waals interaction. Its intercalation properties make titanium disulfide an important material for cathodes in rechargeable batteries. Over the last two decades the electronic structure of TiS_2 has been intensively studied both experimentally [14–16] and theoretically [17–22]. The occupied band structure of TiS_2 is rather well understood. At the same time, in spite of the large number of experimental works on photoemission from TiS_2, there has been only a single attempt [14] to calculate the high energy bands of TiS_2. However, the evanescent part of the complex band structure was not taken into account in that work, which caused an uncertainty in the interpretation of the measurements. The aim of the present work is to provide a band structure interpretation of the observed normal incidence electron transmission spectrum of TiS_2.

The paper is organized as follows. The experimental technique is described in section 2 and the theoretical methodology in section 3. In section 4, we present the experimental electron transmission spectrum of TiS_2 and compare it to our *ab initio* calculations.

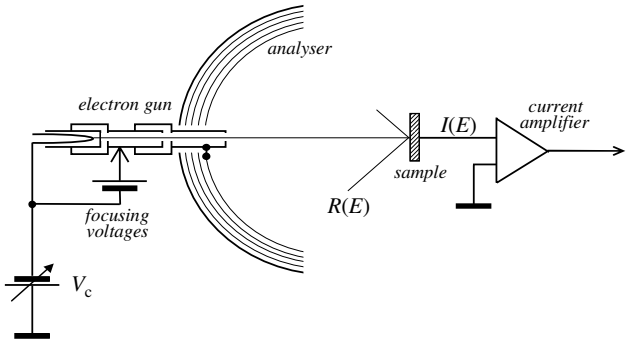

Figure 1. Scheme of the VLEED spectrometer operating in the retarding field mode.

2. Experiment

The experiment was performed with the VLEED spectrometer installed in Chalmers University of Technology, Göteborg, Sweden. Its scheme is shown in figure 1. The spectrometer uses a standard four-grid LEED optics operated in the retarding field mode. In contrast to the standard field-free operation of LEED optics, in this mode the drift tube of the electron gun and the outer grid are disconnected from the ground. A floating power supply delivers to all electrodes of the gun the voltages relative to the cathode as required to extract a well focused electron beam, with the voltage at the last electrode and outer grid connected to it being around +300 V. This forms a retarding field between the gun and the sample kept at the ground potential. Starting from a negative cathode potential V_c, the electrons accelerate in the electron gun and then decelerate on their way to the sample towards their low primary kinetic energy $E = eV_\mathrm{c}$ determined by the cathode potential. In this operation mode very low primary energies can be achieved without any significant degradation in focusing of the electron beam. Moreover, the fact that the electrons travel most of their way to the sample at relatively high energies suppresses the influence of stray magnetic fields. It should be noted that a prerequisite for a well controlled VLEED experiment in the retarding field mode is that the electrostatic masses, such as the manipulator and sample holder, preserve a smooth and symmetric configuration of the electrostatic field. Further details of the experimental technique, including angle-dependent measurements where the retarding field distorts the electron trajectories upon the sample rotation, are described elsewhere [23, 11].

At normal incidence the standard $I(V)$ measurements, when one registers intensities of the diffracted beams on the LEED screen, have a principal limitation that the specular beam falls into the electron gun area and thus escapes detection. Instead, we registered the current in the sample circuit, the technique commonly referred to as target (total, absorbed) current spectroscopy (TCS). This technique is based on the fact that the target current spectrum $I(E)$ is equal to the incident current I_0 minus the total elastic reflectivity $R(E)$ summed over all diffracted beams, and inelastic reflectivity $R_\mathrm{inel}(E)$. (At sufficiently low energies there is only one reflected beam.)

The incident current I_0 is constant, because due to the retarding field operation the focusing voltages on the electrodes of the electron gun are energy independent. The $R_{\rm inel}(E)$ contribution yields only a rather featureless background. Therefore, the $I(E)$ spectrum represents essentially the elastic electron transmission spectrum $T(E) = 1 - R(E)$. In the following, despite the use of the TCS measurement technique, we will refer to the $T(E)$ spectra as VLEED ones in the sense of the dominant physical mechanism forming the spectral structures.

Atomically clean (0001) surfaces of TiS_2 crystals were obtained by standard *in situ* cleavage at a base pressure of 10^{-9} mbar. Observation of LEED patterns with the electron beam scanning across the sample surface showed the presence of minor misoriented crystallites closer to the sample edges, which is typical of layered materials. To ensure clean spectra without contamination from these crystallites, we monitored the LEED patterns during the data acquisition. A beam current about 0.1 μA was sufficient to obtain excellent statistics of the spectra within less than 1 min. Operation at such a low current improved focusing of the beam (the spot size on the sample was <0.5 mm through the whole energy range) as well as allowing operation at reduced cathode temperatures to improve the experimental energy resolution determined by the energy spread of the beam (<0.25 eV HWHM).

3. Theory and computational methodology

The LEED wavefunction Φ is the solution of the Schrödinger equation for a semi-infinite crystal defined by its energy E and the initial conditions of the incident electron, i.e. the asymptotics of the wavefunction in the vacuum. In the plane parallel to the crystal surface Φ obeys the Bloch theorem and is characterized by the 2D Bloch vector $\mathbf{k}_\parallel$. In the vacuum, far from the crystal surface, it is a superposition of plane waves: the plane wave propagating towards the crystal defines incident current, and the total current carried by the LEED state is the transmitted current. The ratio of the two currents is the transmission coefficient $T(E)$. In the absence of inelastic scattering (electron absorption) the crystal half-space is described by a real crystal potential, and the partial waves may be propagating (real $k_\perp$) or evanescent (complex $k_\perp$) Bloch waves. The latter carry zero current, so that $T(E)$ drops to zero when E falls in a $\mathbf{k}_\parallel$-projected band-gap.

In reality, however, owing to inelastic processes, $T(E)$ is always nonzero. Following Slater [24] we take this into account by adding an imaginary term, the optical potential $-\mathrm{i}V_{\rm i}$, to the potential in the crystal half-space. We keep the energy E real, so the absorbing potential leads to a *spatial damping* of the wavefunctions rather than to a decay in time. Then the Bloch vector of an originally propagating wave with a group velocity $v_\perp$ acquires an imaginary part of the order of $V_{\rm i}/\hbar v_\perp$, and the mean free path (MFP) of the electron in the solid is then $\lambda = 1/(2\,\mathrm{Im}\,k_\perp)$. At the same time, in the energy gaps of the propagating spectrum the transmission $T(E)$ is not zero anymore (it should be interpreted as absorption), and the sharp drops and rises of the $T(E)$ function become smooth. The curvature of structures in the $T(E)$ curve can be controlled by the parameter $V_{\rm i}$. By adjusting the shape of the theoretical $T(E)$ curve to the experiment one can construct the energy dependence of $V_{\rm i}$ and, thus, infer about the intensity of inelastic scattering depending on energy.

The phenomenological parameter $V_{\rm i}$ is associated with the expectation value of the imaginary part of the self-energy operator $\Sigma(\mathbf{r}, \mathbf{r}'; E)$ [25]. It may have a complicated real-space structure, which means that different partial waves of the LEED function should, in principle, be ascribed different values of $V_{\rm i}$. The approximation of a spatially constant self-energy may be rather unsatisfactory if the LEED state is composed of several Bloch waves, as has been evidenced in recent studies on photoemission from $TiTe_2$ [26] and aluminium [27]. However, at high energies the Σ operator cannot be reliably calculated by the state-of-the-art methods, and the empirical determination of $V_{\rm i}$ is the only way to quantify inelastic scattering.

In section 4 we shall discuss calculations with $V_{\rm i} \neq 0$. There, depending on the context, we shall use the term real band structure (RBS) both for the band structure of an infinite crystal and for the fragments of the complex band structure that originate from propagating Bloch waves at $V_{\rm i} = 0$. The Bloch waves in the gaps of RBS, which have nonzero $\mathrm{Im}\,k_\perp$ at $V_{\rm i} = 0$, are referred to as genuinely evanescent waves.

3.1. Computational procedure and parameters

Computational procedure starts with constructing self-consistent potentials in the bulk crystal and at the surface. The local density approximation (LDA) of the density functional theory is used. The band structure calculations are performed with the extended linear augmented plane wave method (ELAPW), using the full-potential augmented Fourier components technique described in [28]. Typical computational parameters for layered chalcogenides can be found elsewhere [11, 28]. To determine the potential at the surface a repeated slab calculation was performed. The slab consists of three TiS_2 sandwiches separated by a vacuum region of 16 au; see figure 2. The calculated work function is $\phi = 6.7$ eV, which somewhat overestimates the experimental value of 5.8 eV. This discrepancy is most probably due to the LDA, the accuracy of which we cannot control.

Then for a given energy E the inverse band structure problem is solved, i.e., the partial Bloch waves $\psi_{k_\perp}$ are determined that satisfy the Schrödinger equation $\hat{H}\psi_{k_\perp} = E\psi_{k_\perp}$ in the bulk of the crystal. Owing to the complex potential $-\mathrm{i}V_{\rm i}$ included in the Hamiltonian $\hat{H}$, all the waves have a finite imaginary part of the surface perpendicular component $k_\perp$ of the Bloch vector. The calculations are performed with the ELAPW-$\mathbf{k}\cdot\mathbf{p}$ method, which reduces the inverse band structure problem to a matrix eigenvalue problem, with $k_\perp$ being the eigenvalues; see [3]. To the left from the matching plane $z_{\rm M}$ the LEED function Φ is a linear combination of several $\psi_{k_\perp}$ (only the waves with $\mathrm{Im}\,k_\perp$ not exceeding 1 au^{-1} are included).

Between $z_{\rm M}$ and $z_{\rm V}$ the potential strongly deviates from the periodic potential in the bulk, and it depends on all three coordinates. In the present calculation the embedded region does not include any atomic layers, because for the layered

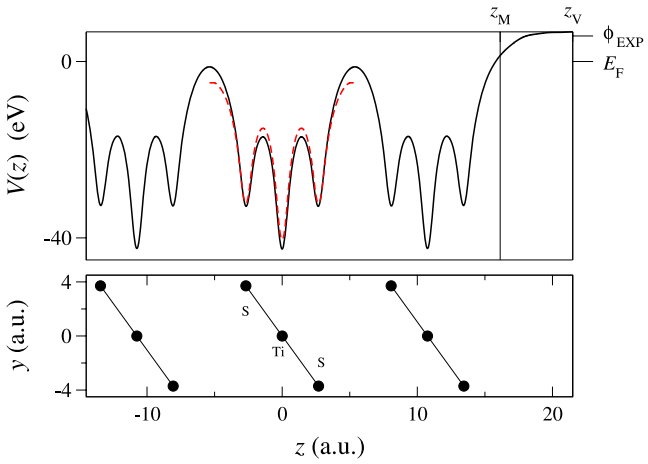

Figure 2. Crystal potential profile $V(z)$ at the surface. For $z < z_M$, it coincides with the potential of the infinite crystal. In the vacuum region, $z > z_V$, the potential is constant. The full potential is shown by the solid line and the muffin-tin potential by the dashed line. The lower panel shows three structure units of three surface layers.

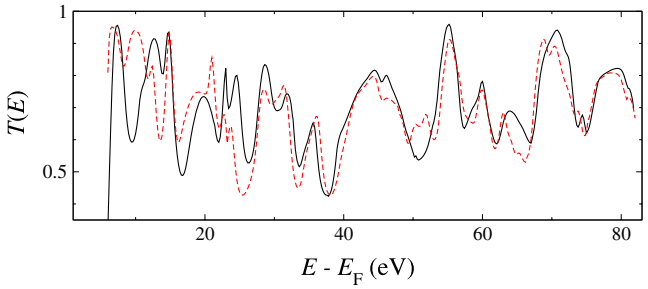

Figure 3. Normal incidence transmission spectra $T(E)$ for $V_i = 0.5$ eV calculated with the full potential (solid line) and with the muffin-tin potential (dashed line).

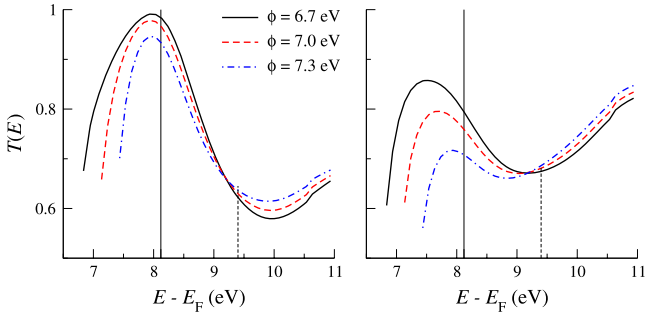

Figure 4. Transmission spectra $T(E)$ calculated with the self-consistent full potential in the bulk for three values of work function, $\phi = 6.7$, 7.0 and 7.3 eV (solid, dashed and dot–dashed curves, respectively). The optical potential is $V_i = 0.6$ eV. The spectra in the left graph are obtained with the smooth *ab initio* potential at the surface, and in the right graph with a step-like potential. The solid vertical line at 8.1 eV shows the location of the experimental maximum and the dashed line at 9.4 eV of the experimental minimum.

structure the potential at the uppermost monolayer is already practically the same as in the bulk. In this region the function Φ is expanded in terms of the eigenfunctions ξ_n of the three-sandwich slab; see [5]. The same set of ξ functions is used for all energies E. In order to accurately describe the energy region up to 40 eV above the Fermi level we included 225 ξ functions with energies up to 55 eV above E_F.

Finally, in the vacuum, Φ is a superposition of plane waves, of which one is the incident wave and the others are reflected or evanescent waves. They play the same role as the functions $\psi_{k_\perp}$ in the bulk. Then, for each energy E the three representations are matched at the two planes z_M and z_V, and a function is constructed that is smoothly continuous at the two planes and satisfies (with a certain accuracy) the equation $\hat{H}\Phi = E\Phi$ in the embedded region. (The Schrödinger equation is satisfied by construction both in the bulk and in the vacuum region.)

3.2. Influence of the exact shape of the potential in the bulk and at the surface

The present method employs the most accurate representation of the wavefunction—augmented plane waves—and provides the same quality of the scattering states as in state-of-the-art band structure calculations. In order to understand whether the achieved accuracy is worth the numerical effort we shall consider two sources of technical difficulties, which in the present method are treated differently than in the KKR method, namely the non-muffin-tin potential in the bulk and the shape of the surface potential barrier.

Although full-potential KKR methods have existed for many years [29] the muffin-tin approximation (MTA) to the crystal potential is still widely used in the theory of LEED [30]. The reason is that the KKR method is especially efficient for muffin-tin potentials. It is instructive to see how the effect of the approximation depends on the kinetic energy. Figure 3 compares the $T(E)$ curve obtained with the full potential with the one calculated within the MTA. The latter is explicitly derived from the former by spherically averaging the potential inside the MT spheres and averaging the potential in the interstitial; see the dashed curve in figure 2. Both calculations employ a step-like surface barrier. The basis set (and, consequently, the numerical accuracy) is the same in both cases, so the difference between the two curves in figure 3 is solely due to the shape of the potential. In spite of the layered (far from close-packed) structure of TiS_2 the MTA turns out to be reasonable at higher kinetic energies. However, its quality rapidly deteriorates below 20 eV.

In the present calculation the surface region, which cannot be included either in the bulk or in the vacuum half-space, is relatively thin, $z_V - z_M = 5$ au; see figure 2. Nevertheless, it requires special treatment, which considerably complicates the computational scheme [5]. Because the embedded region does not contain any singularities (there are no adsorbates or intercalated atoms) it is tempting to replace the smoothly growing potential with a sharp step at z_M. Figure 4 shows that this substantially affects both the shape and absolute values of the electron transmission spectrum over an energy region of several electron volts. Just above the barrier, the step-like potential, as expected, more efficiently reflects electrons: at the maximum, where the transmission is due to the RBS fragment

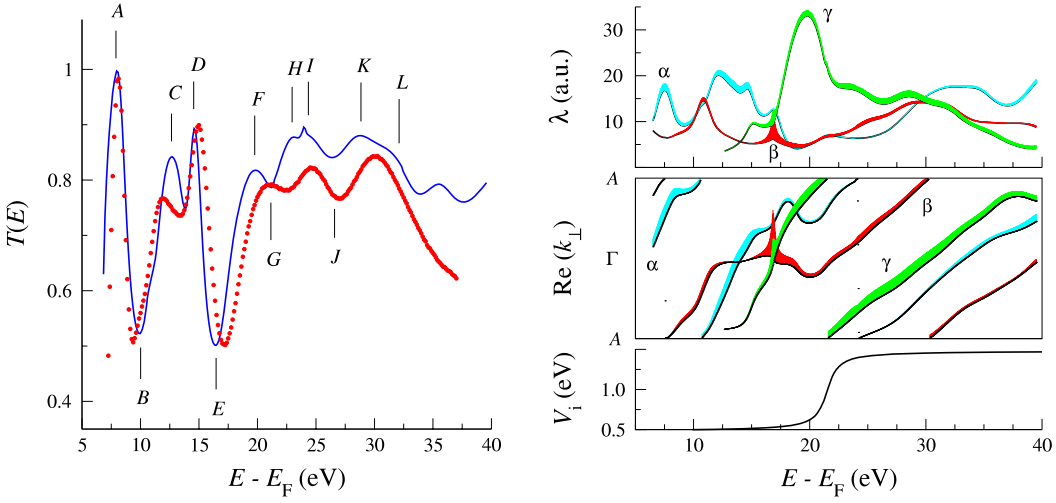

Figure 5. Left: comparison of the experimental (dots) and theoretical (line) normal incidence transmission spectra of TiS_2. Locations of the structures in the theoretical curve are indicated by the vertical bars. Right: energy dependence of the optical potential $V_i(E)$ used in the calculation (lowermost panel), the resulting band structure $E(\mathrm{Re}\,k_\perp)$ (middle panel) and the mean free path $\lambda = (2\,\mathrm{Im}\,k_\perp)^{-1}$ (upper panel) for the three most important CBS branches. The vertical extent of the shaded area shows relative contributions of the branches to the LEED state.

of the branch α (see figure 6), the transmission with the smooth potential is higher than with the abrupt one. At the same time, with the realistic smooth potential, the minimum due to the gap in the real band structure is deeper than with the step-like one, and the transmission above the gap (branch β) is lower. The energy shift of the extrema is about 0.5 eV, which is larger than the possible uncertainty of the measurements or of the numerical procedure. Another interesting observation is that with the smooth potential the $T(E)$ curve is more stable to the variations of the work function than with the step-like potential.

4. Results and discussion

The calculated $T(E)$ spectrum is compared with the measured one in figure 5. The experiment does not provide absolute values of $T(E)$, first because the incident current is difficult to measure, and second because of the unknown background of secondary electrons. Thus, in order to compare the measured $I(E)$ curve with theory the former should be transformed (assuming a constant background b) according to the formula $T_{\mathrm{exp}}(E) = aI(E) + b$. The parameters a and b are determined so as to fit T_{exp} to the theoretical $T(E)$. Because the amplitude of the variations of the calculated $T(E)$ depends on the unknown value of V_i the functions $V_i(E)$ and $T_{\mathrm{exp}}(E)$ are determined self-consistently by an iterative procedure [11].

A rather good agreement between the theory and the experiment has been achieved with the $V_i(E)$ function shown in the right graph of figure 5. It is an arctan curve with the inflection point at 21.5 eV. The value of 21.5 eV was chosen because this is the plasmon energy of TiS_2 [31]. Above this energy the inelastic scattering is expected to become stronger because the electrons can lose enough energy to create plasmons [11]. The measured $T(E)$ variations being much sharper below 21 eV than above this energy is reproduced by a steep increase of V_i by about 0.9 eV. A similar sharp increase of V_i that closely correlates with the plasmon energy has been observed in $NbSe_2$ [11]. We did not observe a step-like behaviour of $V_i(E)$ in $TiTe_2$ [12], perhaps because of the unfavourable location of its plasmon energy relative to the $T(E)$ structures. Another reason for the different behaviour of these similar crystals may be the spatial structure of the self-energy operator mentioned in section 3.

The complex band structure underlying the theoretical $T(E)$ curve is shown in the right panels of figure 5. Three branches are found to strongly contribute to current transmission through the surface. The dispersion of the bands $E(\mathrm{Re}\,k_\perp)$ is seen to be far from the free-electron parabola often assumed in interpreting photoelectron spectra. Also the behaviour of the mean free path is very different from the universal U-shaped curve often cited in the literature [32].

In order to interpret the origin of the structures in the $T(E)$ curve we present in figure 6 a detailed band structure analysis of the normal incidence target current. In the lower panel we show a $T(E)$ spectrum for $V_i = 0.25$ eV. With this unphysically small value the structures are seen more clearly, and the connection of the conducting complex band structure to the real band structure of the infinite crystal is more transparent. The latter is shown in the central panel by the thin lines. The lines of variable thickness depict the three most important conducting branches of the CBS. The thickness of the line is proportional to the current carried (absorbed) by the individual partial wave.

Because in the absorbing medium the current is not conserved, the analogue of current is the integral of the density distribution in the LEED state over the absorbing half-space [33, 10]:

$$T_{\mathrm{bulk}} = \frac{2V_i}{\hbar} \int_{\mathrm{bulk}} |\Phi(\mathbf{r})|^2 \,\mathrm{d}\mathbf{r}. \qquad (1)$$

If Φ is an exact solution of the Schrödinger equation then T_{bulk} equals the current in the right half-space, where $V_i = 0$ and current is conserved. The partial currents $T_{k_\perp}$ are calculated

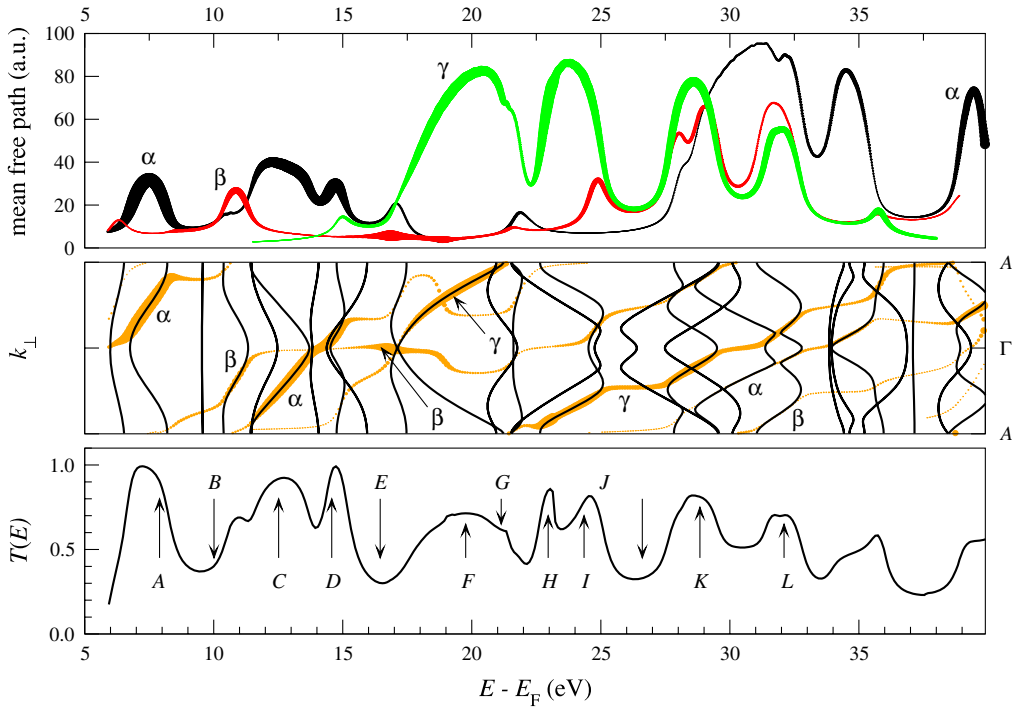

Figure 6. Band structure analysis of the normal incidence electron transmission in TiS_2. Lowest panel: transmission spectra $T(E)$ for $V_i = 0.25$ eV. Middle panel: real band structure in the AΓA interval (thin lines) superimposed on the complex band structure for $V_i = 0.25$ eV. The three real lines of the CBS that most strongly contribute to the transmitted current are shown. They are labelled by α, β and γ. The thickness of the line is proportional to the current carried by the individual partial wave. The imaginary part of the complex wavevectors can be inferred from the upper panel. Upper panel: dependence of the mean free path λ on energy for the conducting CBS branches. The thickness of the line is proportional to the current carried by the wave.

by equation (1) for each $\psi_{k_\perp}$ that constitutes Φ. In the limit $V_i \to 0$ the expression (1) reduces to the usual expression for a current in an elastic (nonabsorbing) medium, and the functions $\psi_{k_\perp}$ obey the orthogonality condition: current carried by a superposition of Bloch eigenfunctions of the same energy is the sum of the individual currents. This is not the case for $V_i \neq 0$, which should be kept in mind when considering figure 6.

The simplest interpretation of minima and maxima in the $T(E)$ curve which can be arrived at without an explicit calculation of the LEED function is the following: the minimum occurs in a gap of the real band structure, which is spanned by a CBS line connecting two bands through the complex $k_\perp$ plane, the CBS line being responsible for the absorption of the current when $V_i \neq 0$. The maximum corresponds to an RBS line, and it occurs close to the point where the group velocity and, consequently, the mean free path is maximal.

In the upper panel of figure 6 the energy dependence of the mean free path $\lambda = (2\ \mathrm{Im}\, k_\perp)^{-1}$ is shown for the three branches that substantially contribute to the LEED state. They are denoted by α, β and γ. The maxima A, C, D, F and K are in perfect accord with the above interpretation. In contrast, the maxima H and I occur in the same RBS fragment belonging to branch γ, the peak H being to the left and I to the right from the MFP maximum. At larger values of V_i the two peaks merge into one broad maximum, so the double structure is not resolved experimentally.

The structure of the minimum B at 10 eV also does not completely fit into the above simple scheme. Its shape is affected by a narrow conducting RBS fragment of branch β, which falls at 11 eV into the 3 eV wide RBS gap of branch α. The minimum E at 16.5 eV is even more complicated: just at this energy the current carrying branch switches from α to γ, and around the minimum the current is absorbed by branch β. The structure of branch β is rather unusual: it spans a very wide gap between 11.5 and 20.5 eV. It is interesting that at 17 eV, apart from the evanescent wave belonging to β, there exist two RBS members from α and γ with much larger values of MFP. Nevertheless, their contribution to Φ is much smaller than that of the rapidly decaying β wave. The minimum at 30.5 eV is another example when the transmission is due to a genuinely evanescent wave with a short MFP (branch γ), although a slowly decaying wave (from the RBS fragment of α) is available. At the maximum L all three waves are propagating at $V_i = 0$, but the main contribution is from γ, which has the shortest MFP.

The above analysis shows that the transmission role of bulk partial waves cannot in general be inferred from their integral properties, such as group velocity or decay rate. At the same time, in spite of the complicated unoccupied band structure of TiS_2, only three branches determine the transmission over a wide energy range.

5. Conclusions

We have measured the normal incidence VLEED spectrum of the (0001) surface of 1T TiS_2 in the target current mode and explained it by an *ab initio* calculation. We have shown

how the structures of the transmission spectrum can be traced back to the complex band structure of the semi-infinite crystal. Based on a very good agreement between experiment and theory in the energy location of the TCS structures over the whole interval, we explain the observed shape of the spectra by the energy dependence of the optical potential.

The most interesting feature of the normal incidence transmission of TiS_2 is the broad minimum at 17 eV where the main current carrying wave switches from one branch to another. (We have not encountered such behaviour in our previous studies on layered crystals [11, 12, 10].) Our results suggest that this energy region might be especially interesting for photoemission measurements because the photoelectron escape depth (which is the mean free path of the LEED theory) changes very rapidly with the final state energy and reaches extremely small values at the minimum.

The present study further reinforces the idea that complex band structure is an efficient paradigm for interpreting electron diffraction. Being the most direct probe of unoccupied electron states, VLEED proves an indispensable complement to photoelectron spectroscopy. The presented theoretical description, which emphasizes the connection of VLEED with unoccupied band structure, can be equally applied to secondary electron emission (SEE) because, as shown theoretically [34] and experimentally [35], the SEE spectra are equivalent to the VLEED transmission spectra on top of a featureless background due to cascade electrons.

Acknowledgment

This work was supported in part by Ikerbasque—Basque Foundation for Science.

References

[1] Heine V 1963 *Proc. Phys. Soc.* **81** 300
Heine V 1964 *Surf. Sci.* **2** 1
[2] Pendry J B 1969 *J. Phys. C: Solid State Phys.* C **2** 2273
[3] Krasovskii E E and Schattke W 1997 *Phys. Rev.* B **56** 12874
[4] Krasovskii E E and Schattke W 1999 *Phys. Rev.* B **59** 15609
[5] Krasovskii E E 2004 *Phys. Rev.* B **70** 245322
[6] Pendry J B 1974 *Low Energy Electron Diffraction* (London: Academic)
[7] Pendry J B 1976 *Surf. Sci.* **57** 679
[8] Feibelman P J and Eastman D E 1974 *Phys. Rev.* B **10** 4932
[9] Strocov V N 2003 *J. Electron Spectrosc. Relat. Phenom.* **130** 65
[10] Barrett N, Krasovskii E E, Themlin J-M and Strocov V M 2005 *Phys. Rev.* B **71** 035427
[11] Krasovskii E E, Schattke W, Strocov V N and Claessen R 2002 *Phys. Rev.* B **66** 235403
[12] Strocov V N, Krasovskii E E, Schattke W, Barrett N, Berger H, Schrupp D and Claessen R 2006 *Phys. Rev.* B **74** 195125
[13] Wilson J A and Yoffe A D 1969 *Adv. Phys.* **18** 193
[14] Strocov V N, Starnberg H, Nilsson P O, Brauer H E and Holleboom L J 1997 *J. Phys.: Condens. Matter* **10** 5749
[15] Matsushita T, Suga S, Kimura A, Negishi H and Inoue M 1999 *Phys. Rev.* B **60** 1678
[16] Kimura A, Negishi H, Inoue M, Matsushita T, Saitoh Y, Imada S and Suga S 2007 *Phys. Rev.* B **76** 235102
[17] Zunger A and Freeman A J 1977 *Phys. Rev.* B **16** 906
[18] Benesh G A, Woolley A M and Umrigar C 1985 *J. Phys. C: Solid State Phys.* **18** 1595
[19] Fang C M, de Groot R A and Haas C 1997 *Phys. Rev.* B **56** 4455
[20] Sharma S, Nautiyal T, Singh G S, Auluck S, Blaha P and Ambrosch-Draxl C 1999 *Phys. Rev.* B **59** 14833
[21] Reshak A H and Auluck S 2003 *Phys. Rev.* B **68** 245113
[22] Reshak A H, Kityk I V and Auluck S 2008 *J. Chem. Phys.* **129** 074706
[23] Strocov V N 1996 *Meas. Sci. Technol.* **7** 1636
[24] Slater J C 1937 *Phys. Rev.* **51** 840
[25] Silkin V M, Chulkov E V and Echenique P M 2003 *Phys. Rev.* B **68** 205106
[26] Krasovskii E E, Rossnagel K, Fedorov A, Schattke W and Kipp L 2007 *Phys. Rev. Lett.* **98** 217604
[27] Krasovskii E E, Schattke W, Jiříček P, Vondráček M, Krasovska O V, Antonov V N, Shpak A P and Bartoš I 2008 *Phys. Rev.* B **78** 165406
[28] Krasovskii E E, Starrost F and Schattke W 1999 *Phys. Rev.* B **59** 10504
[29] Butler W H, Gonis A and Zhang X-G 1992 *Phys. Rev.* B **45** 11527
Zeller R 1997 *Phys. Rev.* B **55** 9400
[30] Rundgren J 2003 *Phys. Rev.* B **68** 125405
[31] Buslaps T 1992 unpublished
[32] Van Hove M A, Weinberg W H and Chan C-M 1986 *Low-Energy Electron Diffraction* (*Springer Series in Surface Sciences* vol 6) (Berlin: Springer)
[33] Strocov V N, Starnberg H I and Nilsson P O 1997 *Phys. Rev.* B **56** 1717
[34] Feder R and Pendry J B 1978 *Solid State Commun.* **26** 519
[35] Bovet M, Strocov V N, Clerc F, Koitzsch C, Naumovic D and Aebi P 2004 *Phys. Rev. Lett.* **93** 107601